Supporting Information

Construction of cobalt oxyhydroxide nanosheets with rich oxygen vacancies as high-performance lithium-ion batteries anodes

Yonghuan Fu,‡[a] Liewu Li,‡[ab] Shenghua Ye,[a] Penggang Yang,[a] Peng Liao,[d] Xiangzhong Ren,[a] Chuanxin He,[a] Qianling Zhang*[a] and Jianhong Liu*[ac]

[a]Graphene Composite Research Center, College of Chemistry and Environmental Engineering, Shenzhen University, Shenzhen, 518060, P. R. China

[b]College of Physics and Optoelectronic Engineering, Shenzhen University, Shenzhen, 518060, China

[c]Shenzhen Eigen-Equation Graphene Technology Co. Ltd, Shenzhen, 518000, P. R. China

[d]Department of Cell Research and Development, Farasis Energy Inc., Hayward, California, 94545, USA

***E-mail address of the corresponding author: zhql@szu.edu.cn; liujh@szu.edu.cn**

‡Yonghuan Fu and Liewu Li contributed equally to this work.

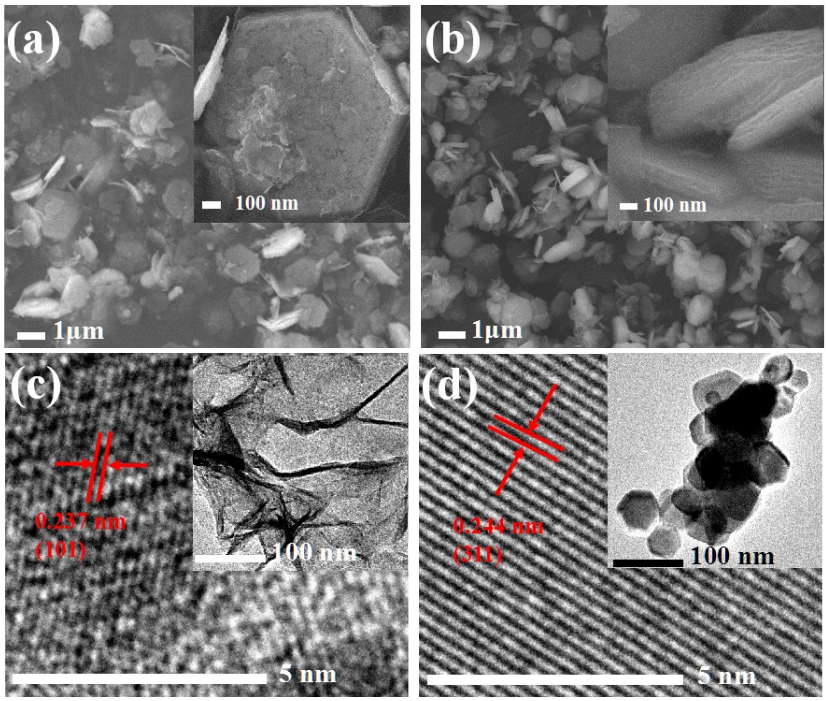

Fig. S1 SEM images of $Co(OH)_2$ (a) and Co_3O_4 (b); TEM images of $Co(OH)_2$ (c) and Co_3O_4 (d).

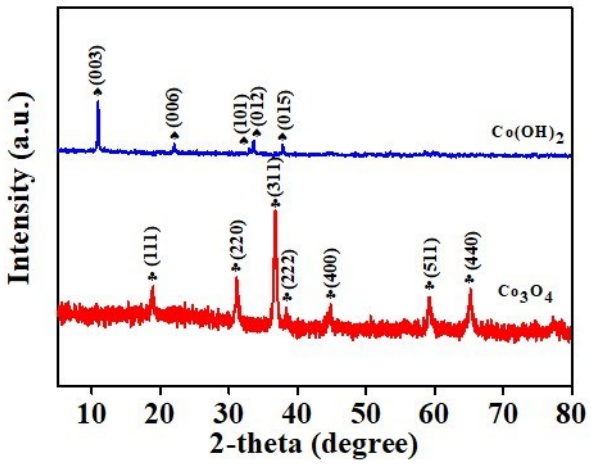

Fig. S2 XRD patterns of $Co(OH)_2$ and Co_3O_4.

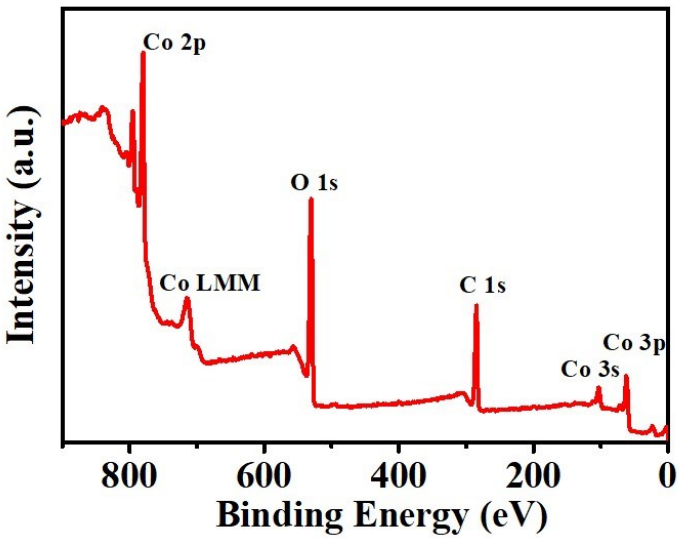

Fig. S3 XPS spectrum of CoOOH nanosheets.

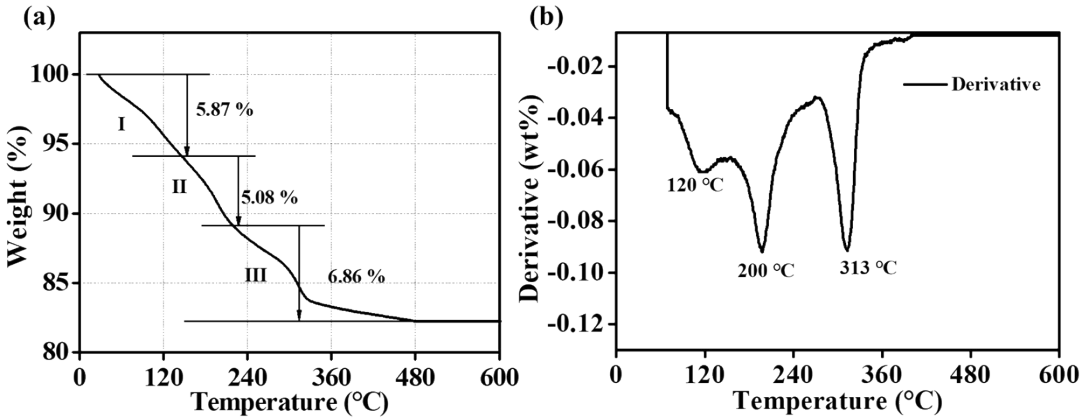

Fig. S4 (a) TG profile of CoOOH nanosheets; (b) TGA profile of CoOOH nanosheets.

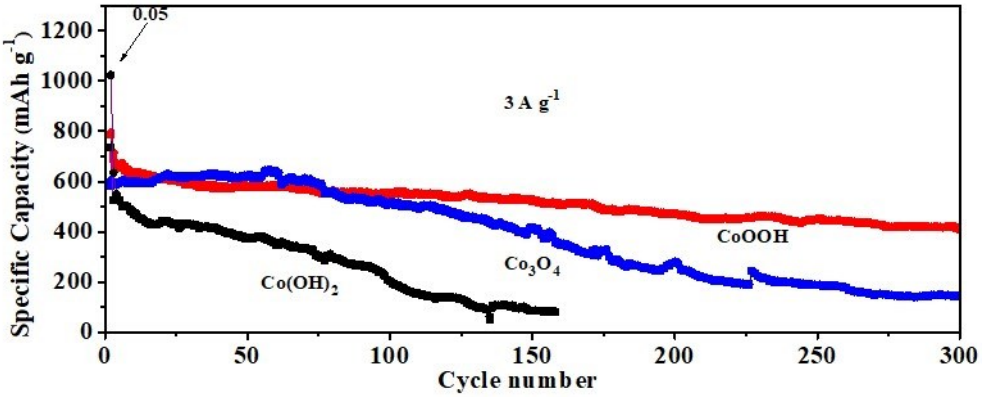

Fig. S5 Cycling performance of CoOOH, $Co(OH)_2$, and Co_3O_4 electrodes at 3 A g^{-1}.

Table S1. Comparison of cycling stability and initial coulombic efficiency of CoOOH anode with previously reported cobalt oxide anodes for LIBs.

Anode materials	Current density ($mA\ g^{-1}$)	Cycle number	Capacity retention ($mAh\ g^{-1}$)	Initial coulombic efficiency (%)	Refs
Co_3O_4 nanosheets	200	100	1717	~68	[1]
CoOOH in Lithium–Sulfur Battery	0.1C (about 100)	100	1199.4	--	[2]
The composite materials of mica flake and cobalt oxide	225	70	650	--	[3]
The yolk–shell Co_3O_4/C	200	120	1100	~71	[4]
N-Doped Carbon/Cobalt Ferrite Hybrid Nanocomposites	3000	300	410	~78	[5]
Nanoarchitectured Co_3O_4/reduced graphene oxide	1C(about 1000)	200	513.9	--	[6]
Co_3O_4 nanotubes	100	80	380	~58.7	[7]
nanoparticles-assembled Co_3O_4 microspheres	200	50	1340	~73	[8]
Oxidizing solid Co into hollow Co_3O_4	200	500	871.5	~66.7	[9]
$Co_2(OH)_2CO_3$ nanowires and rGO films	200	150	1380	~71.7	[10]
CoOOH nanosheets	200	300	1588	~90	This work

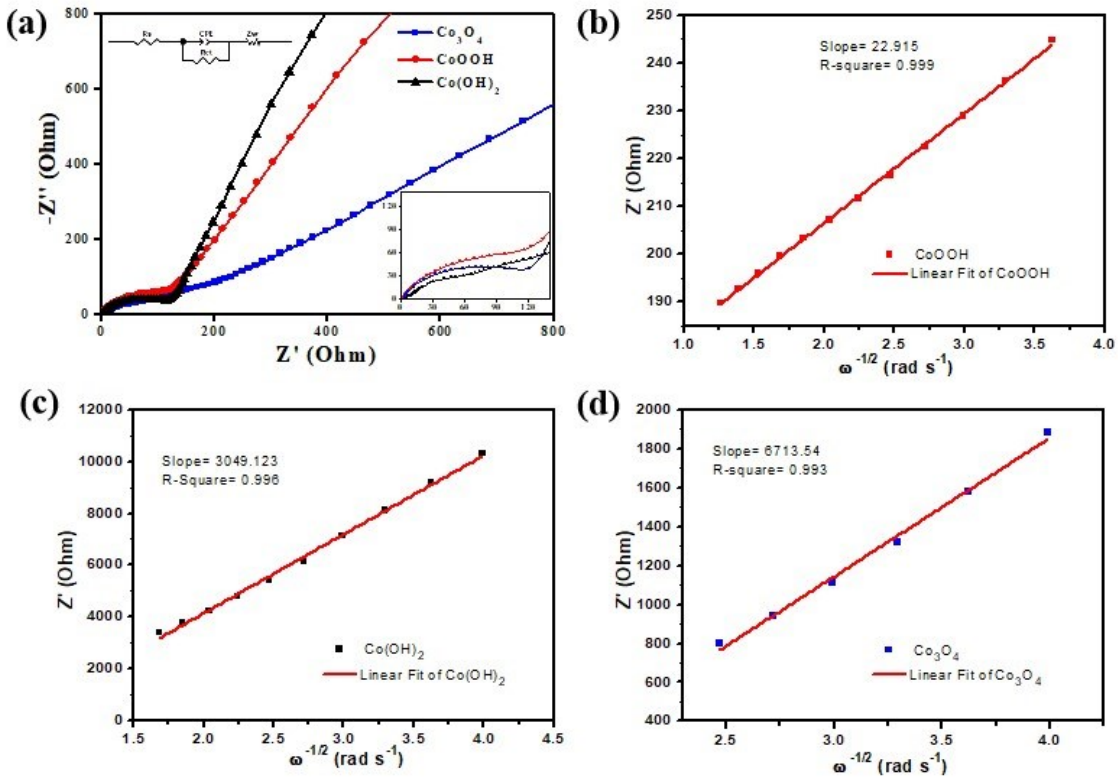

Fig. S6 (a) Nyquist plots of CoOOH, $Co(OH)_2$, and Co_3O_4 electrodes (insets show the equivalent circuits for EIS fitting and the detail of Nyquist plots); (b) The relationship between I_{peak} and $v^{1/2}$ for CoOOH electrode; (c) The relationship between I_{peak} and $v^{1/2}$ for $Co(OH)_2$ electrode; (d) The relationship between I_{peak} and $v^{1/2}$ for Co_3O_4 electrode.

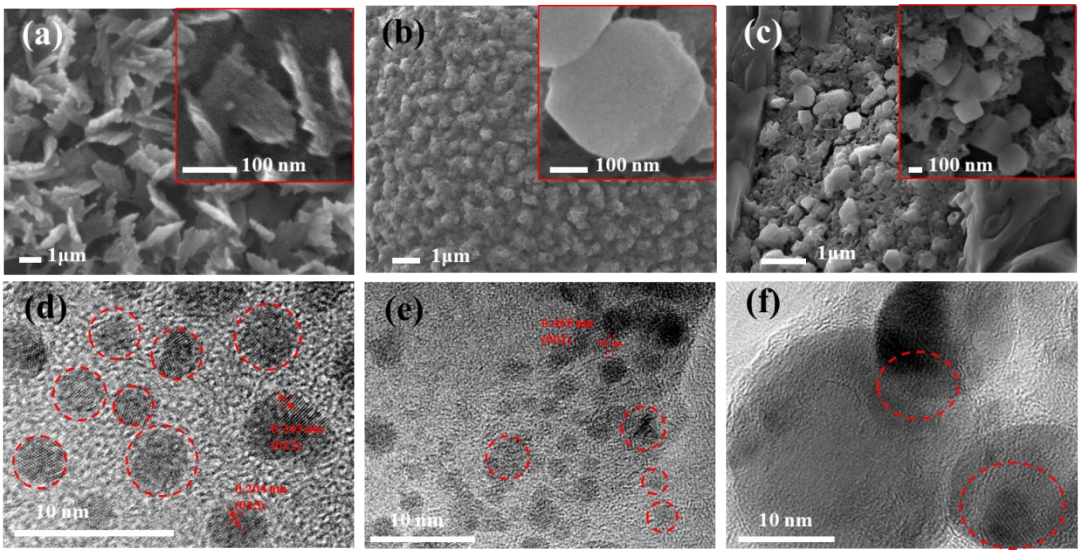

Fig. S7 SEM and High-resolution TEM images of CoOOH (a, d), $Co(OH)_2$ (b, e), and Co_3O_4 (c, f) electrodes after 300 cycles.

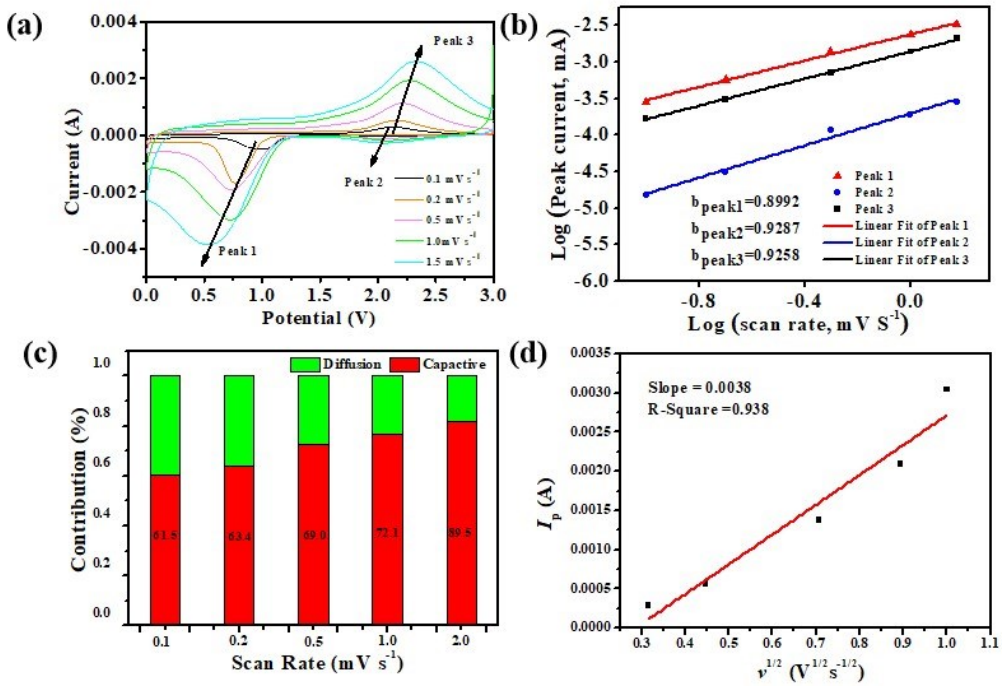

Fig. S8 Kinetic analysis of the electrochemical behavior of the Co_3O_4 electrode versus Li^+/Li. (a) CV curves at various scan rates ranging from 0.1 to 1.5 mV s^{-1}; (b) Determination of b values using the relationship between the peak current and scan rate according to the voltammograms in (a); (c) Contribution ratios of the capacitive and diffusion-controlled effects at various scan rates; (d) The relationship between I_p and $v^{1/2}$.

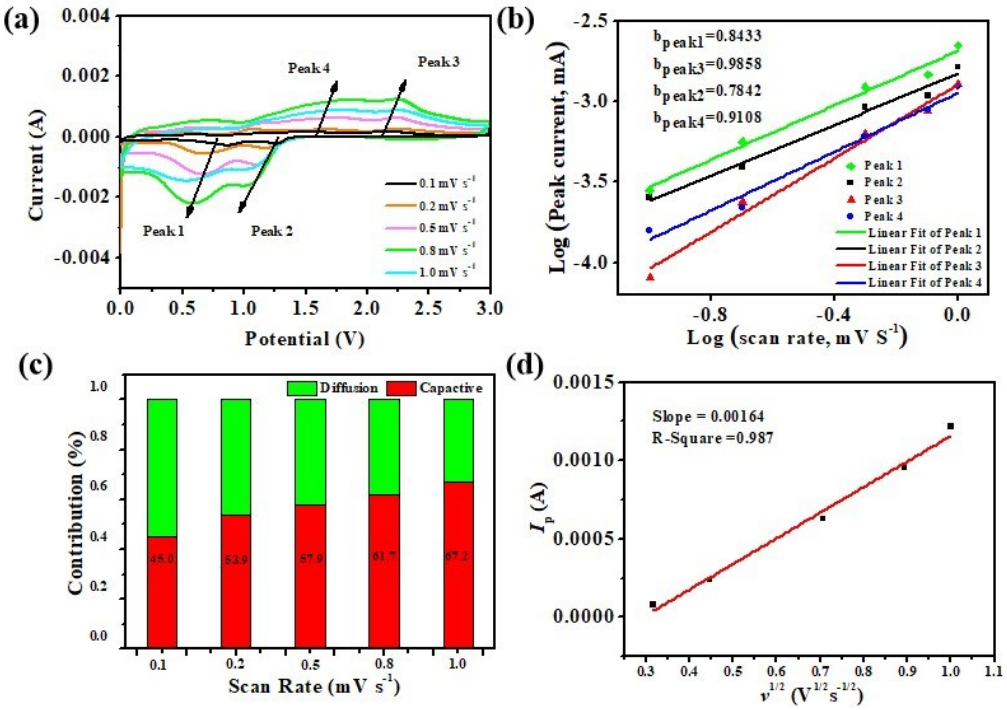

Fig. S9 Kinetic analysis of the electrochemical behavior of the $Co(OH)_2$ electrode versus Li^+/Li. (a) CV curves at various scan rates ranging from 0.1 to 1.0 mV s^{-1}; (b) Determination of b values using the relationship between the peak current and scan rate according to the voltammograms in (a); (c) Contribution ratios of the capacitive and diffusion-controlled effects at various scan rates; (d) The relationship between I_p and $v^{1/2}$.

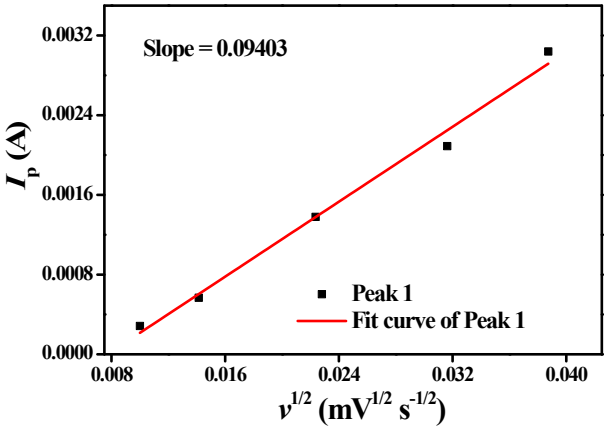

Fig. S10 The relationship between I_p and $v^{1/2}$ for the CoOOH electrode.

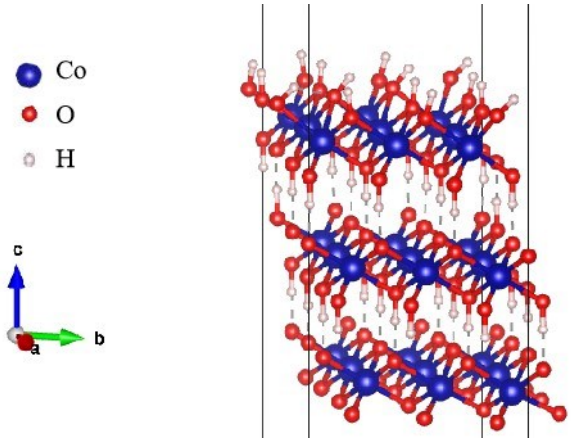

Fig. S11 A 3 × 3 supercell of the CoOOH (001) crystal surface including 3 atomic layers model.

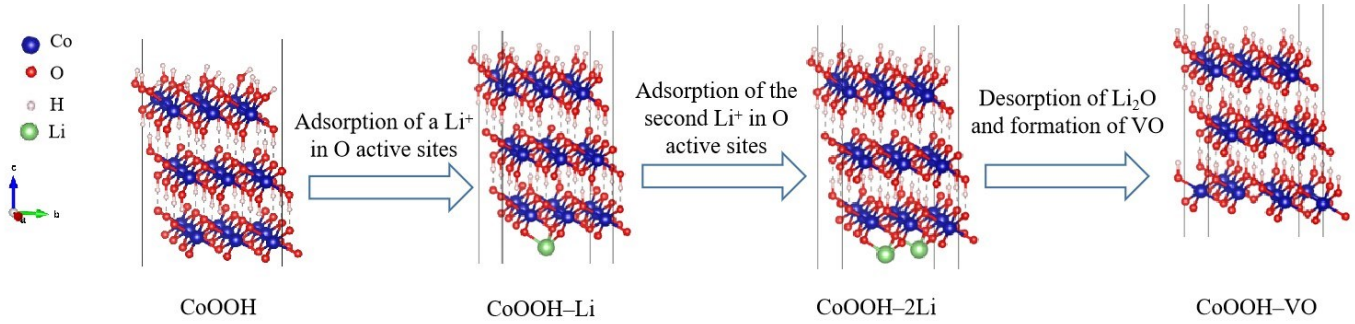

Fig. S12 The model of the process for adsorption of Li^+ in O active sites, desorption of Li_2O and formation of VO.

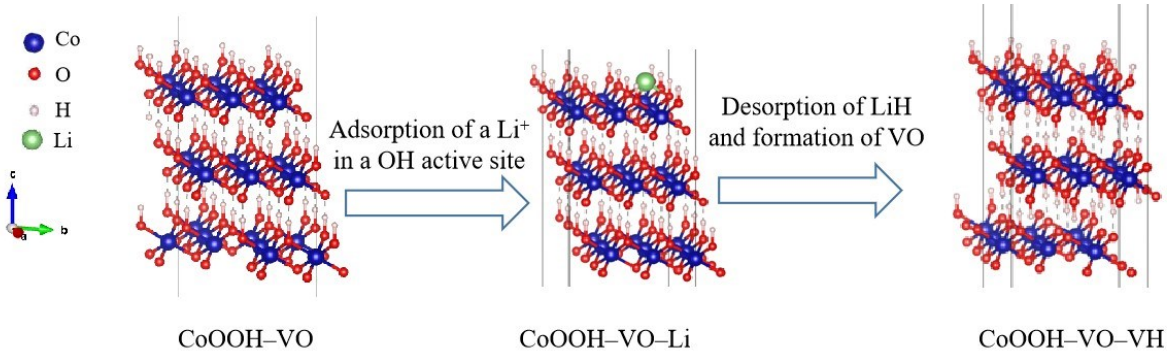

Fig. S13 The model of the process for adsorption of Li^+ in a OH active site and formation of LiH or LiOH; desorption of LiH and formation of CoOOH–VO–VH.

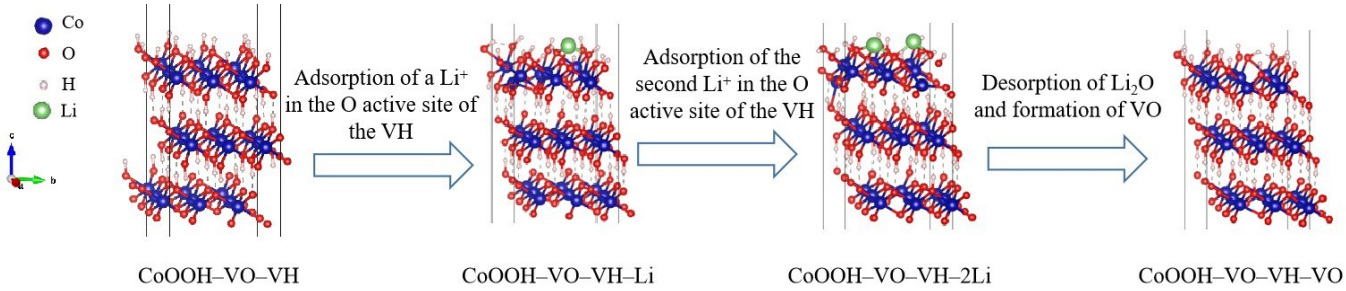

Fig. S14 The model of the process for adsorption of Li^+ in the O active site of the VH; desorption of Li_2O and formation of CoOOH–VO–VH–VO.

References

1. R. Wei, X. Zhou, T. Zhou, J. Hu and J. C. Ho, *J. Phys. Chem. C.*, 2017, **121**, 19002-19009.

2. Z. Y. Wang, L. Wang, S. Liu, G. R. Li and X. P. Gao, *Adv. Funct. Mater.*, 2019, **29**, 1901051.

3. L. Kong, J. Lang, M. Liu, Y. Luo and L. Kang, *J. Power Sources*, 2009, **194**, 1194-1201.

4. Y. Wu, J. Meng, Q. Li, C. Niu, X. Wang, W. Yang, W. Li and L. Mai, *Nano Res.*, 2017, **10**, 2364-2376.

5. N. Dang, T. Nguyen, E. Lizundia, T. Le and M. J. MacLachlan, *ChemistrySelect*, 2020, 5, 8207-8217.

6. Z. Chen, Y. Gao, X. Chen, B. Xing, C. Zhang, S. Wang, T. Liu, Y. Liu and Z. Zhang, *Ionics*, 2019, **25**, 5779-5786.

7. X. Lou, D. Deng, J. Lee, J. Feng and L. A. Archer, *Adv. Mater.*, 2008, **20**, 258-262.

8. T. Li, X. Li, Z. Wang, H. Guo, Q. Hu and W. Peng, *Electrochim. Acta*, 2016, **209**, 456-463.

9. J. Wang, H. Wang, F. Li, S. Xie, G. Xu, Y. She, M. K. H. Leung and T. Liu, *J. Mater. Chem. A.*, 2019, **7**, 3024-3030.

10. Y. Dong, Y. Ma, Y. Li, M. Niu, J. Yang, X. Song, D. Li, Y. Liu and J. Zhang, *Nanoscale*, 2019, **11**, 21180-21187.